Concrete behavior in steel-concrete-steel panels subjected to biaxial tension compression

Manish Prasad, Cheng-Jun Huang, Xiao-Bing Song *, Si-Jia Chen, Chen-Hui Qian

Department of Civil Engineering, Shanghai Jiao Tong University, Shanghai 200240, PR China

ABSTRACT

Steel-Concrete-Steel (SCS) composite wall is being used for different purposes for its improved performances. Some analytical and finite element models have been presented in the past to predict the behavior of such walls. In this paper, an attempt is made to develop an iterative membrane model to analyze SCS wall panels subjected to in-plane membrane forces in the principal directions. The model accounts for the post-cracking Poisson effects of concrete as the Zhu/Hsu ratio.

Individual behaviors of concrete and steel plates in an SCS panel are studied in which confinement in principal tensile direction accompanied by negative uniaxial tensile strain in concrete is observed. To explain this behavior, a detailed perspective for uniaxial strain in principal tensile direction is proposed and the conventional stress-strain trajectory of concrete in tension is extended to incorporate any confinement developed in the concrete. Constitutive law of concrete in compression is also modified to incorporate the observed confining behavior of the concrete.

1. Introduction

An SCS is a steel plate reinforced concrete in which concrete is sandwiched in between two steel plates. In general, SCS does not have vertical or horizontal rebar reinforcements. Steel face plates are connected with the core concrete by regularly spaced flat-headed shear studs. Face steel plates are also connected with each other by cross tie bars.

An SCS structure has improved strength and applicability as prefab over conventional reinforced concrete structures (RC). It was mainly implemented in nuclear power plants during its early development, however, with its popularity, nowadays, high rise buildings, offshore structures [1], and many other structures implement SCS.

To analyze an SCS wall, modeling for concrete has always been one of the major tasks. Various approaches have been put forward to predict the behaviors of concrete in RC panels. Softened Membrane Model (SMM) [2], by Zhu and Hsu, is one of the most accurate and efficient iterative models for cracked RC panels under shear. SMM implements a smeared crack concept, in which cracked concrete is treated as a continuous material, to measure the post-cracking Poisson effect of reinforced concrete. Based on the results of 12 full-scale RC panels, Zhu and Hsu proposed a Zhu/Hsu ratio to characterize the Poisson effect after cracking. Zhu/Hsu ratio was observed to reach an unusual value of 1.9 in the post-yield range. Implementation of the Zhu/Hsu enabled prediction of the post-peak shear behavior of RC panels.

For the past few decades, few models have been proposed to analyses SCS panels. Ozaki et al. [3] gave a truss analogy model at post-cracking behavior incorporating the post-cracking stiffness of concrete and yield strength of the steel plates as described by von-Mises yielding criterion. Suzuki et al. [4] presented an analytical truss model, similar to Ozaki et al. [3] formulation, combined with an arch mechanism which accounts for concrete struts and steel ties remaining from truss mechanism to estimate the shear strength of H-shaped SCS wall. H. Varma et al. [5] formulated a mechanics-based model (MBM) to predict the behavior of the SCS wall subjected to in-plane membrane forces. The MBM did not consider the concrete post-cracking in tension, concrete inelasticity in compression and steel plate post-yielding behaviors. Rectifying the limitations of the MBM, they also presented a non-linear inelastic finite element model that can predict the behavior of SCS walls with reasonable accuracy. Vecchio and McQuade [6] also developed a non-linear inelastic finite element model using Distributed Stress Field Model [7] which accounts for post-cracking poisson ratio of concrete, elastic offset strains due to thermal expansion and shrinkage and plastic offset strains due to yielding, loading history and damage of the material.

The scope of this paper arises from the findings of the experiment of nine SCS panels [8] under uniform biaxial loading, which showed unexpected compressive stress in concrete in principal tensile direction and enlarged peak stress and strain of concrete in compression due to the confinement of concrete provided by the steel faceplates. However, this behavior of concrete was not explained after the yielding of the

steel plate. To explain the post yielding behavior, detailed modeling of concrete under confinement in an SCS panel was required.

So far, all of the models presented are concerned with the overall experimental behavior of an SCS wall. As per this research, the experimental stress state of individual components of an SCS has not been discussed yet. Even though some of the models such as Vecchio and McQuade's model [6] and Varma et al.'s model [5] for SCS account for concrete post-cracking behavior in tension, researches lack the modeling of concrete behavior in tension which can justify the observed compressive stress in Huang et al. [8] experiment. The post-cracking Poisson effects of concrete have also not been given much consideration. Vecchio and McQuade's [6] analytical model does consider the post cracking Poisson ratio but is limited to a value of 0.5 at compressive stress near failure. Despite not including these considerations, most of the previous models can predict the overall SCS behavior with reasonable accuracy. However, modeling of these complex nuances can improve our understating of individual behaviors of concrete and steel plate and can also improve the accuracy in predicting the overall behavior of an SCS panel.

In this paper, to attain the stated objectives, constitutive law of concrete in compression used in SMM will be modified and an appropriate model for the concrete behavior in tension under confinement will be derived empirically to incorporate the observed behavior of SCS panels from the experiments. Post cracking Poisson ratio in the form of the Zhu/Hsu ratio, Eq. (1), and plastic flow of steel plates after yielding under biaxial loading are also taken into consideration. Finally, an iterative procedure is adopted to solve for the unknowns.

$$\nu_{12} = \begin{cases} 0.2 + 850\varepsilon_1 & \text{before yielding} \\ 1.9 & \text{after yielding} \end{cases} \quad (1)$$

where ε_1 is the strain in the steel bars which yields first.

2. Experimental program

Under this experimental program, nine SCS panels were tested, which were subjected to uniaxial tension and compression, and biaxial tension-compression in-plane loadings [8]. Details of the test specimen are shown in Fig. 3. To ensure a uniform distribution of applied forces, the specimens were designed with three major zones: a right and a left horizontal tension transfer zones, an upper and a lower vertical compression transfer zones, and a middle test zone of 800 mm × 800 mm. The reinforcement ratio ρ, the pitch of the studs to steel plate thickness ratio (B_s/t_s), and applied Compression to the Tension load ratio were selected as test parameters which are tabulated in Table 1. Steels with more than 20% ultimate strain and concrete with

150 mm × 150 mm cube strength of about 40 MPa were used. 8 mm diameter and 60 mm long shear studs at an interval of 75 mm were used to connect faceplates with the core concrete, and 10 mm diameter tie bars at an interval of 150 mm were used to connect faceplates with each other. Steel plates are provided with laser cut holes in which shear studs and tie bars are put in place and then welded from outside. Shear studs extend from one plate into the concrete but do not touch the other plate. The tie bars connect the two steel plates together into a module, which also acts as a formwork, into which concrete can be poured at the site.

The test apparatus, as shown in Fig. 1, was designed to simulate a uniform distribution of in-plane uniaxial and biaxial loads. Four different loading modes, Fig. 2, were adopted to load. (See Fig. 10.)

9 SCS specimens as presented in Table 1. For biaxial loading, a proportional loading was adopted which was achieved by a small increment of load in one direction while keeping the load constant in the perpendicular direction. A sequential loading involved proportional loading followed by constant tension loading.

3. Experimental individual behavior of concrete and steel in SCS

In order to study the mechanical behavior of the SCS panel, the results of the nine SCS panels subjected to biaxial tension-compression were used. Major data obtained was the average strain of the panel in principal directions which coincides with the applied force directions. The first task in the process was to obtain the individual stress-strain trajectory of the core concrete and the steel plate.

Fig. 4 shows a membrane SCS panel subjected to average normal stresses σ_1 and σ_2 in 1 and 2-directions respectively and can be separated into a concrete element and a steel plate element. The normal stresses on the concrete element are σ_1^c and σ_2^c, and that on steel plate

Table 1
Test specimen [8].

Specimen	Concrete fcu (MPa)	Steel plate ts (mm)	Steel plate fy (MPa)	Steel plate ratio (ρt)	Bs/ts	Load increment ratio ($\Delta C/\Delta T$)	Load modes
S3–10	42	2.95	310	1.14%	25.4	−1/0	U.C.
S6–10	41	6	275	2.31%	12.5	−1/0	
S3–51	42	2.95	310	1.14%	25.4	−5.2/1	P.S.
S5–41	41	4.75	300	1.83%	15.8	−3.7/1	
S6–41	41	6	275	2.31%	12.5	−3.5/1	
S6–81	41	6	275	2.31%	12.5	−8/1	
S5–11	41	4.75	300	1.83%	15.8	−1/1	S- P.S.-C.
S6–21	41	6	275	2.31%	12.5	−1.8/1	
S6–01	41	6	275	2.31%	12.5	0/1	U.T.

Note: U.C.—Uniaxial compression.
P.S.—Proportional loading in stepped increment.
S—P.S.—C.—Sequential loading.
U.T.—Uniaxial tension.

Fig. 1. Load setup and testing apparatus [8].
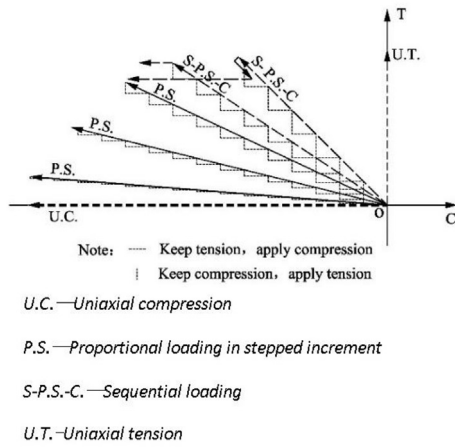
Fig. 2. Loading modes [8].

element are $\rho\sigma_1^s$ and $\rho\sigma_2^s$. All stresses are expressed as equivalent stress which is the stress equal to the stress on a concrete element of equivalent thickness. The coefficient of equivalence used to define the concrete equivalence to steel is taken as ρ and termed as reinforcement ratio. ε_1 and ε_2 denotes the average strain of the panel, ε_1^s and ε_2^s denotes the average strain of the steel plate, and ε_1^c and ε_2^c denotes the average strain of

the concrete measures in 1 and 2-directions respectively. An average strain is a strain measured over several cracks.

Steel plate has a well-defined stress-strain relationship, however, that of concrete is always uncertain. With known mechanical behavior of steel plate and load-deformation curve of the SCS panels obtained from the experiment, the behavior of core concrete could be predicted with an appropriate approach. For the preceding purpose, an incremental model, satisfying all three principals of mechanics of materials, was adopted to calculate the stress state of concrete in an SCS panel.

For SCS panel [8], as shown in Fig. 4, the applied stress coordinate, principal coordinate of the applied stresses, and principal coordinate of the concrete stresses coincide. Therefore, all equations from Eqs. (2) to (14) are established on the basis of principal 1–2 coordinate. Supposing $t_c/(t_c + 2t_s) = 1$, equilibrium equations can be established as Eqs. (2) and (3).

3.1. Equilibrium equations

$$\sigma_1^c = \sigma_1 - \rho\sigma_1^s \tag{2}$$

$$\sigma_2^c = \sigma_2 - \rho\sigma_2^s \tag{3}$$

where $\rho = 2t_s/t_c$ is the steel plate ratio
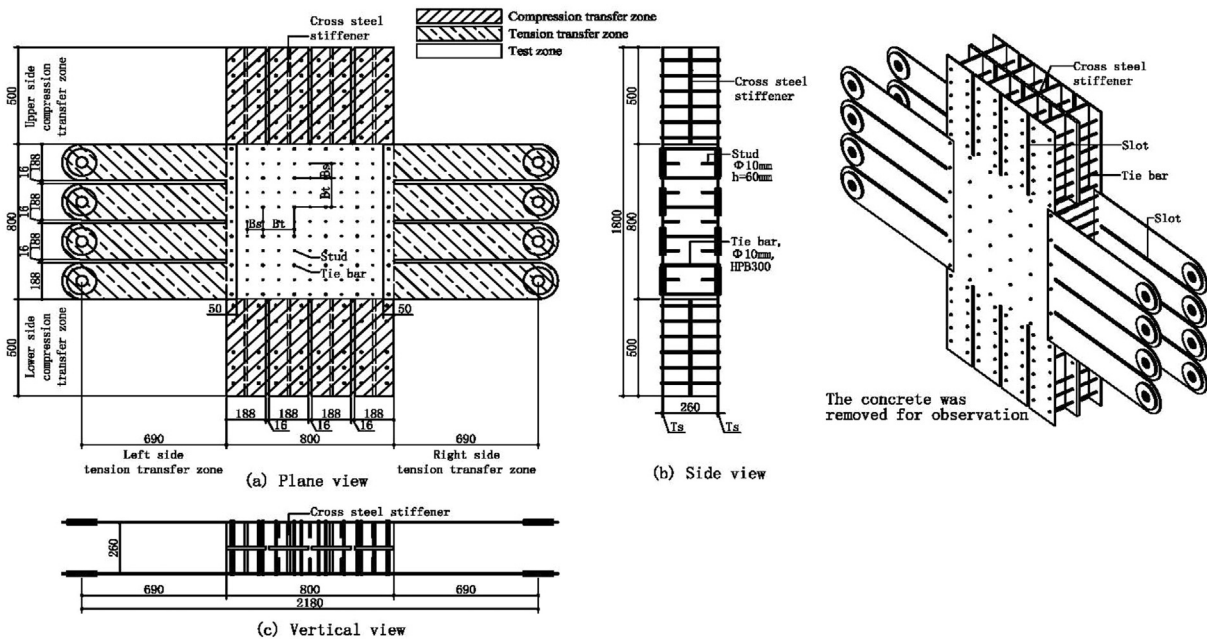
Fig. 3. SCS Specimen properties [8].
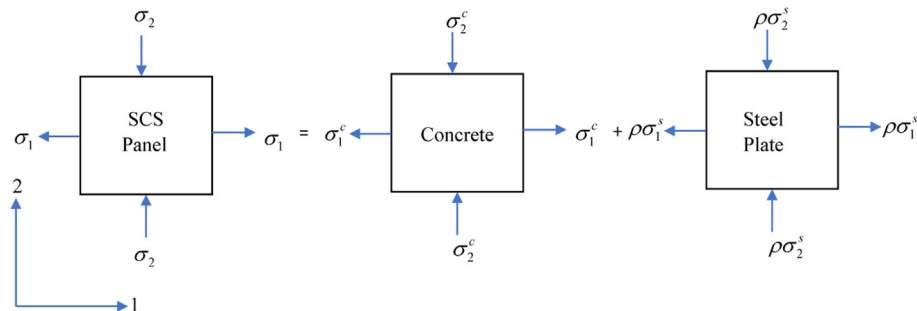
Fig. 4. Individual stress state of SCS panel, core concrete, and steel plate.
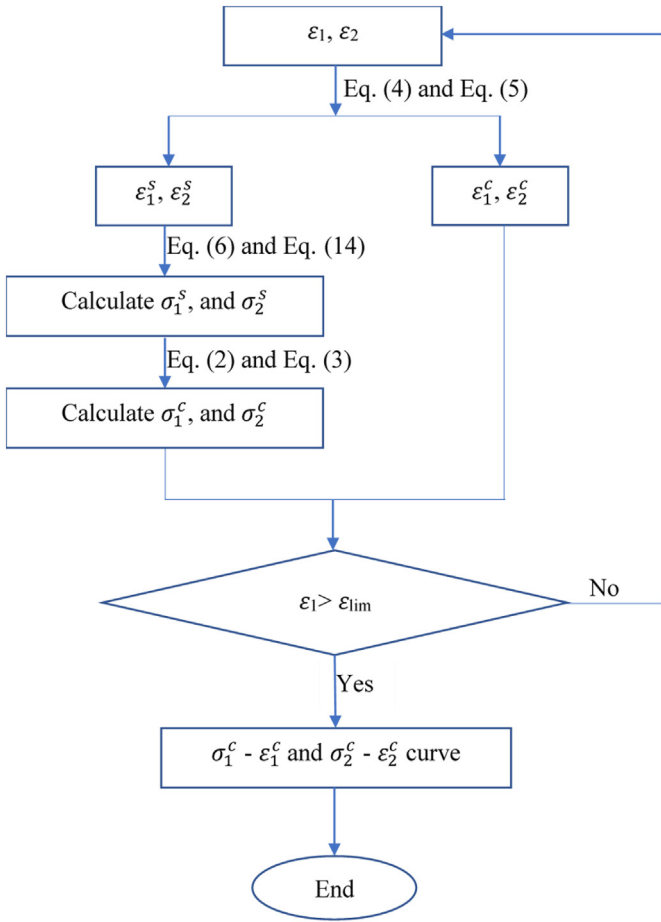
Fig. 5. Flow chart of solution procedure to attain experimental individual behavior of concrete and steel in SCS.

3.2. Compatibility equations

$$\varepsilon_1 = \varepsilon_1^c = \varepsilon_1^s \tag{4}$$

$$\varepsilon_2 = \varepsilon_2^c = \varepsilon_2^s \tag{5}$$

3.3. Constitutive laws of steel plate

A linear stress-strain relationship, Eq. (6), has been used for the steel plate before yielding, when total strain is equal to the elastic strain. However, after yielding, the total strain also incorporates plastic strain and is expressed in Eq. (7) in incremental form. The plastic strain increment $d\varepsilon_{ij}^p$ can be obtained using the associated flow rule [16], Eq. (9), where f is the von-Mises yield surface expressed by Eq. (8). Using Eqs. (6) to (9), Eq.(10) can be obtained and can be rearranged as Eq. (11). Yet undetermined scalar quantity $d\lambda$ can be obtained from consistency condition, Eq. (12), which states that for elastic-perfectly

plastic material, stress state stays on the yield surface during plastic deformation. Using the consistency condition in Eq. (11) gives $d\lambda$ as Eq. (13). Finally, substituting $d\lambda$ back in Eq. (11) yields Eq. (14), which is the desired stress-strain relationship for steel plate after yielding for plane stress state.

$$\begin{Bmatrix} d\sigma_1 \\ d\sigma_2 \end{Bmatrix} = \left\{ \frac{E}{1-\nu^2} \begin{bmatrix} 1 & \nu \\ \nu & 1 \end{bmatrix} \right\} \begin{Bmatrix} d\varepsilon_1 \\ d\varepsilon_2 \end{Bmatrix} \tag{6}$$

$$d\varepsilon_{ij} = d\varepsilon_{ij}^e + d\varepsilon_{ij}^p \tag{7}$$

$$f = \sqrt{J_2} - k = 0 \tag{8}$$

where J_2 is the second invariant of deviatoric stress and k is a material constant.

$$d\varepsilon_{ij}^p = d\lambda \frac{\partial f}{\partial \sigma_{ij}} = d\lambda s_{ij} \tag{9}$$

where $d\lambda$ is a non-negative scalar quantity, σ_{ij} is the stress tensor, and s_{ij} is deviatoric stress tensor.

$$\begin{Bmatrix} d\sigma_1 \\ d\sigma_2 \end{Bmatrix} = \frac{E}{1-\nu^2} \begin{bmatrix} 1 & \nu \\ \nu & 1 \end{bmatrix} \left(\begin{Bmatrix} d\varepsilon_1 \\ d\varepsilon_2 \end{Bmatrix} - d\lambda \begin{Bmatrix} s_1 \\ s_2 \end{Bmatrix} \right) \tag{10}$$

$$\begin{Bmatrix} d\sigma_1 \\ d\sigma_2 \end{Bmatrix} = \frac{E}{1-\nu^2} \begin{bmatrix} 1 & \nu \\ \nu & 1 \end{bmatrix} \begin{Bmatrix} d\varepsilon_1 \\ d\varepsilon_2 \end{Bmatrix} - d\lambda \begin{Bmatrix} t_1 \\ t_2 \end{Bmatrix} \tag{11}$$

where $t_1 = \frac{E}{1-\nu^2}(s_1 + \nu s_2)$ and $t_2 = \frac{E}{1-\nu^2}(s_2 + \nu s_1)$

$$df = \frac{\partial f}{\partial \sigma_{ij}} d\sigma_{ij} = s_{ij} d\sigma_{ij} = 0 \tag{12}$$

$$d\lambda = \frac{1}{s} [t_1 \; t_2] \begin{Bmatrix} d\varepsilon_1 \\ d\varepsilon_2 \end{Bmatrix} \tag{13}$$

where $s = s_1 t_1 + s_2 t_2$

$$\begin{Bmatrix} d\sigma_1 \\ d\sigma_2 \end{Bmatrix} = \left\{ \frac{E}{1-\nu^2} \begin{bmatrix} 1 & \nu \\ \nu & 1 \end{bmatrix} - \frac{1}{s} \begin{bmatrix} t_1^2 & t_1 t_2 \\ t_1 t_2 & t_2^2 \end{bmatrix} \right\} \begin{Bmatrix} d\varepsilon_1 \\ d\varepsilon_2 \end{Bmatrix} \tag{14}$$

Using an incremental step analysis, Fig. 5, involving Eqs. (2) to (6) and Eq. (14), the individual stress-strain trajectory of concrete and steel plate components of each panel were obtained as shown in Figure 12Figure 13 by dotted lines. This result will be used to compare the result of an SCS analysis procedure presented next in the paper.

4. The average Poisson effect in core concrete

Concrete under compression in one direction produces strain in the perpendicular direction. This phenomenon can be predicted by a well-known Poisson ratio of about 0.2 but, after cracking, it becomes discontinuous and the phenomenon becomes very erratic. However, SMM
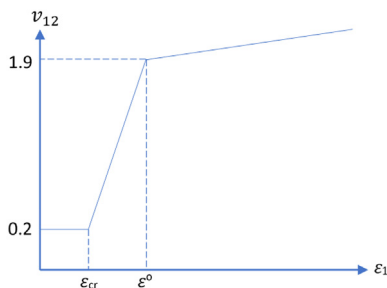
Fig. 6. A modified Zhu/Hsu ratio v_{12}.
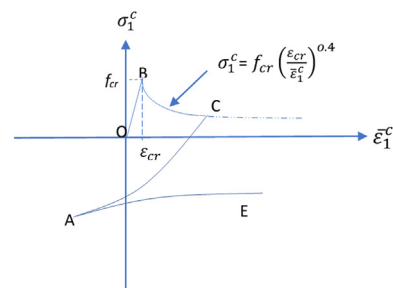
Fig. 7. Uniaxial stress-strain relationship of concrete in tension.
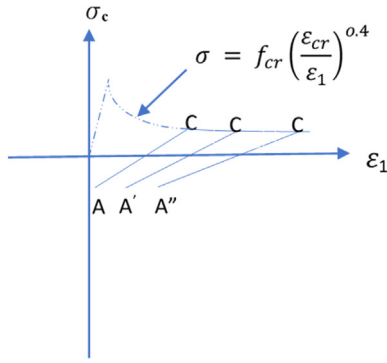
Fig. 8. Illustration of the uniaxial stress-strain stiffness computation method.

Fig. 9. Chart for triaxial compressive strength of concrete [13].

being based on the smeared crack concept, it treats concrete as a continuous material even after cracking. Thus, the average value of the Poisson effect can be measured over several cracks as Zhu/Hsu, Eq. (1). The Zhu/Hsu ratio was in fact measured for RC panels and SMM uses it as for concrete. It might have been assumed that Zhu/Hsu ratio measured for the RC panel can be used for plain concrete. This assumption was based on the results of 12 full-sized RC panels [9], which had shown that Zhu/Hsu ratios were not a function of the reinforcement ratio in RC. Despite of not being dependent on reinforcement, change in the behavior of the Zhu/Hsu ratio was shown dependent on yielding of reinforcement as in Eq. (1). Even though such an assumption led to very accurate results, it is not reasonable to relate any behavior of the concrete material to any other material property but itself. Hence, Zhu/Hsu ratio is modified to be related to a damage parameter ε^o instead of reinforcement property because the change in the behavior of v_{12} with the degree of damage in concrete is more general and reasonable. A modified expression for v_{12} is presented in Fig. 6 and as Eq. (15).

$$v_{12} = \begin{cases} 0.2 & \varepsilon_1 \leq \varepsilon_{cr} \\ 0.2 + 1889(\varepsilon_1 - \varepsilon_{cr}) & \varepsilon_{cr} < \varepsilon_1 \leq \varepsilon^o \\ 1.9 + 80(\varepsilon_1 - \varepsilon^o) & \varepsilon_1 > \varepsilon^o \end{cases} \quad (15)$$

$$v_{21} = \begin{cases} 0.2, & \varepsilon_1 \leq \varepsilon_{cr} \\ 0, & \varepsilon_1 > \varepsilon_{cr} \end{cases} \quad (16)$$

where v_{12} = ratio of smeared strain increment of concrete in tensile direction due to the strain increment in compressive direction to smeared strain increment of concrete in compressive direction,

v_{21} = ratio of smeared strain increment of concrete in compressive direction due to the strain increment in tensile direction to the smeared strain increment of concrete in tensile direction,

ε^o = concrete damage parameter taken as 0.001.

ε_{cr} = cracking strain taken as 0.0001 mm/mm.

In Fig. 6, the Poisson effect remains constant before cracking. After cracking, as the load increases, the severity of cracks also increases, resulting in increased v_{12} and can be measured as a function of ε_1. With increasing applied load, the damage of the concrete also increases but the rate of the formation of new cracks slows down. With higher compressive load concrete may behave like an individual column, and bear load without any significant cracking and eventually start crushing after peak load. So, when certain damage is reached in concrete, represented by ε^o, cracks are assumed to be saturated and cannot increase significantly and therefore, v_{12} is assumed to increase with a gentle slope. v_{21} remains constant at 0.2 before cracking and assumed to be zero after cracking as expressed in Eq. (16).

Biaxial strains ε_1 and ε_2 can be expressed as Eqs. (17) and (18). Solving Eqs. (17) and (18) gives Eqs. (19) and (20), which can be used to determine the uniaxial strains. Hsu and Mo. [10] defined uniaxial strain as
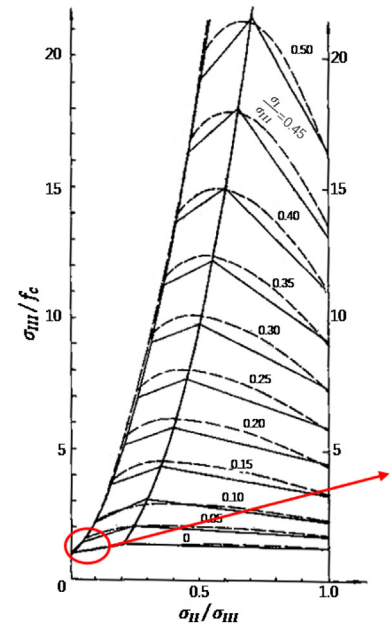
smeared strain in the principal coordinate of applied stress, when a panel is subjected to uniaxial loading with Zhu/Hsu ratio in consideration or as the biaxial strain without Zhu/Hsu ration into consideration. This was the uniaxial strain for both the concrete and the panel. This definition was made for RC panel which has very less confinement provided by the reinforcement. However, when the confinement is significant, the uniaxial strains for the concrete and that of the panel may not be the same. So, a more unified definition should be put forward for the uniaxial strain for concrete itself. A proper definition of uniaxial strains is presented in the latter section.

$$\varepsilon_1 = \bar{\varepsilon}_1^c - v_{12}\bar{\varepsilon}_2^c \quad (17)$$

$$\varepsilon_2 = \bar{\varepsilon}_2^c - v_{21}\bar{\varepsilon}_1^c \quad (18)$$

$$\bar{\varepsilon}_1^c = \frac{1}{1 - v_{12}v_{21}}\varepsilon_1 + \frac{v_{12}}{1 - v_{12}v_{21}}\varepsilon_2 \quad (19)$$

$$\bar{\varepsilon}_2^c = \frac{v_{21}}{1 - v_{12}v_{21}}\varepsilon_1 + \frac{1}{1 - v_{12}v_{21}}\varepsilon_2 \quad (20)$$
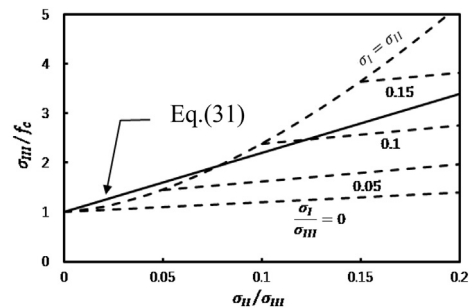
Fig. 10. Approximation of triaxial chart for biaxial stress state [13].
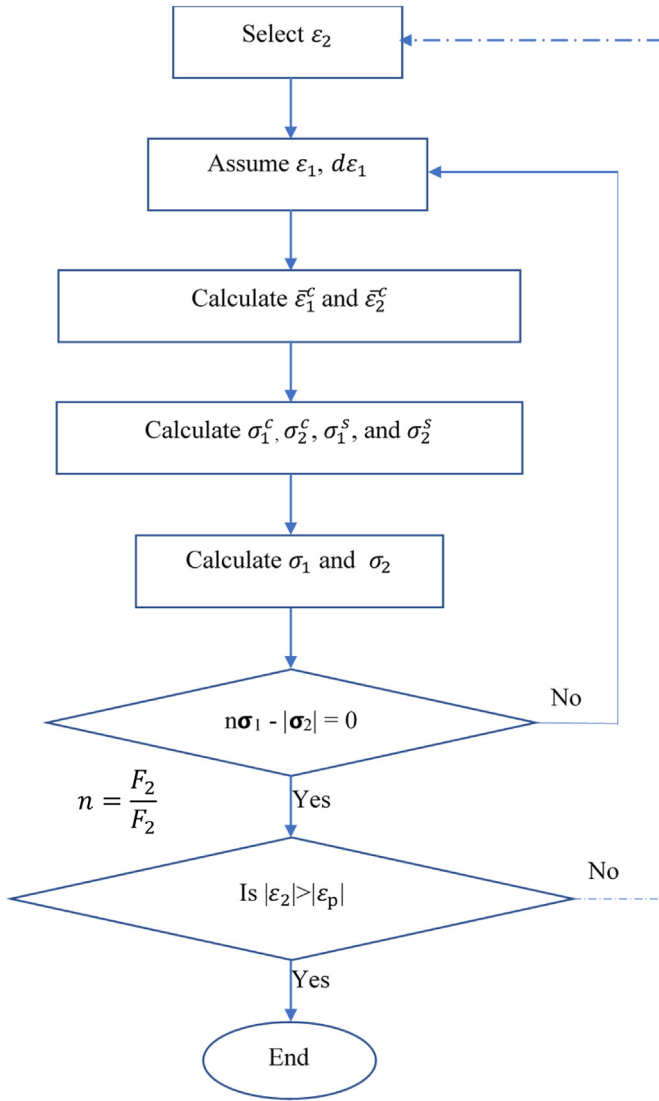
Fig. 11. Flow chart of solution procedure of SCS Membrane Model.

5. Constitutive laws of concrete

5.1. Concrete in tension

Fig. 7 shows a complete uniaxial stress-strain trajectory for concrete in tension. A unique and contrasting behavior has been observed after cracking which is explained henceforth.

5.1.1. The uniaxial strain $\bar{\varepsilon}_1^c$

Conventional uniaxial stress-strain relationships of concrete in RC do not account for the confinement. It is interesting to note that the uniaxial strain may not always increase with the increase in ε_1 when concrete is under significant confinement. Compatibility of steel plate and concrete can produce a significant amount of confinement and can vary with the change in the property of either concrete or steel plate or both. So, if there is confinement, it can restrict the expansion of concrete but increasing confinement can also produce a compressive strain. With the variation of developed confinement in concrete, the uniaxial strain in direction-1 can also vary. To understand this behavior, the uniaxial strain is decomposed into two parts as in Eq. (21). When ε_1^T dominates, uniaxial strain increases and when ε_1^{cf} dominates, uniaxial strain decreases.

A typical example of increasing and decreasing behavior of $\bar{\varepsilon}_1^c$ is illustrated in Fig. 7. Before yielding, the confinement provided by the steel plate is more effective, hence a bigger ε_1^{cf} which causes the uniaxial strain to decrease. Whereas the effectiveness decreases after yielding, hence a relatively smaller ε_1^{cf} which causes an increase in uniaxial strain. This results in increasing compressive stress before yielding and decreasing compressive stress after yielding in the principal tensile direction. And, the total tensile strain is the sum of uniaxial strain and the strain caused by the strain in perpendicular direction-2, which is expressed as Eq. (22).

$$\bar{\varepsilon}_1^c = \varepsilon_1^T + \varepsilon_1^{cf} \tag{21}$$

$$\varepsilon_1 = \bar{\varepsilon}_1^c + \varepsilon_1^C \tag{22}$$

where ε_1^T = tensile strain in direction-1($+$ve) caused by the applied tensile load without considering the Zhu/Hsu ratio

ε_1^{cf} = compressive strain in direction-1($-$ve) caused by the confinement

ε_1^C = strain in direction-1 caused by the strain in direction-2

This behavior of uniaxial strain of concrete under confinement may be difficult to observe in an experiment because it is the average strain developed in concrete due to the combined effect of applied stress and developed confinement in the principal tensile direction. Therefore, uniaxial tensile strain $\bar{\varepsilon}_1^c$ should be defined as the strain variation in direction-1 caused by the stress variation in the same direction.

5.1.2. Before cracking

Concrete is isotropic with a known Poisson ratio of 0.2 and a linear stress-strain relationship Eq. (23) as proposed by Belarbi and Hsu [11] and Pang and Hsu [12] can be adopted.

$$\sigma_1^c = E_c \bar{\varepsilon}_1^c \tag{23}$$

where, $E_c = 3875\sqrt{f_c'(MPa)}$, modulus of elasticity of concrete

5.1.3. After cracking

Concrete is discontinuous and treated as an orthotropic material. So, the conventional value of 0.2 as the Poisson ratio cannot be used and the average Poisson ratio in both directions also changes. As cracks are parallel to principal direction 2, v_{21} is assumed to be zero. However, v_{12} keeps increasing with the severity of cracks. As v_{12} is in the range of 0.2 to 0.3, any increase in compressive strain produces a smaller concrete tensile strain in direction-1 than that of steel which has a Poisson ratio of 0.3. This causes additional tensile stress in concrete because of the compatibility condition. This might cause an accelerated cracking of the concrete. The uniaxial stress-strain relationship is expressed as proposed by Belarbi and Hsu [11] and Pang and Hsu [12] which follows Eq. (24). This equation represents the curve BC in Fig. 7.

$$\sigma_1^c = f_{cr}\left(\frac{\varepsilon_{cr}}{\bar{\varepsilon}_1^c}\right)^{0.4} \tag{24}$$

where ε_{cr} = cracking strain of concrete and f_{cr} = cracking stress of concrete

When v_{12} increases beyond the Poisson ratio of the steel plate, 0.3 before yielding and about 0.5 after yielding, an increase in compressive strain produces a larger concrete tensile strain in direction-1 than that of steel. This larger strain produced in the tensile direction gets confined by the steel plates due to the compatibility condition. This confinement caused by the steel plates develops compressive stress on the concrete and can be termed as confining stress. When the strain ε_1^{cf} caused by the confining stress overcomes the strain ε_1^T caused by applied tensile stress, the uniaxial tensile strain may commence decreasing. This particular condition was observed as shown by point C in Fig. 7. This is
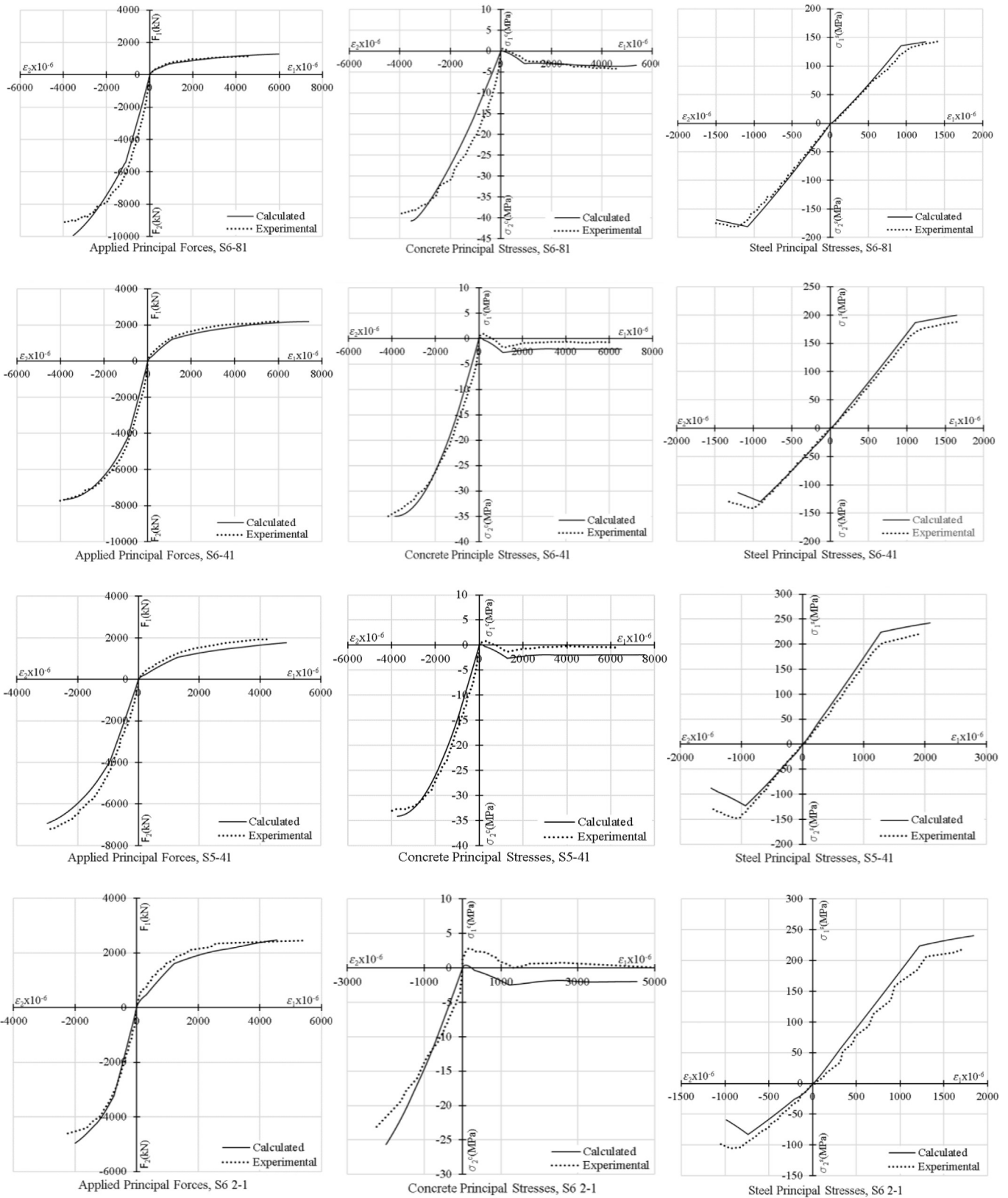
Fig. 12. Comparison of experimental and calculated results.

analogous to the unloading of the concrete in the tensile direction.

$$\sigma_c = f_{cr}\left(\frac{\varepsilon_{cr}}{\overline{\varepsilon}_1^c}\right)^{0.4} \tag{25}$$

$$E_{cr} = -0.4 f_{cr} \frac{\varepsilon_{cr}^{0.4}}{\varepsilon_1^{1.4}} \tag{26}$$

where, E_{cr} is the stiffness of the cracked concrete.
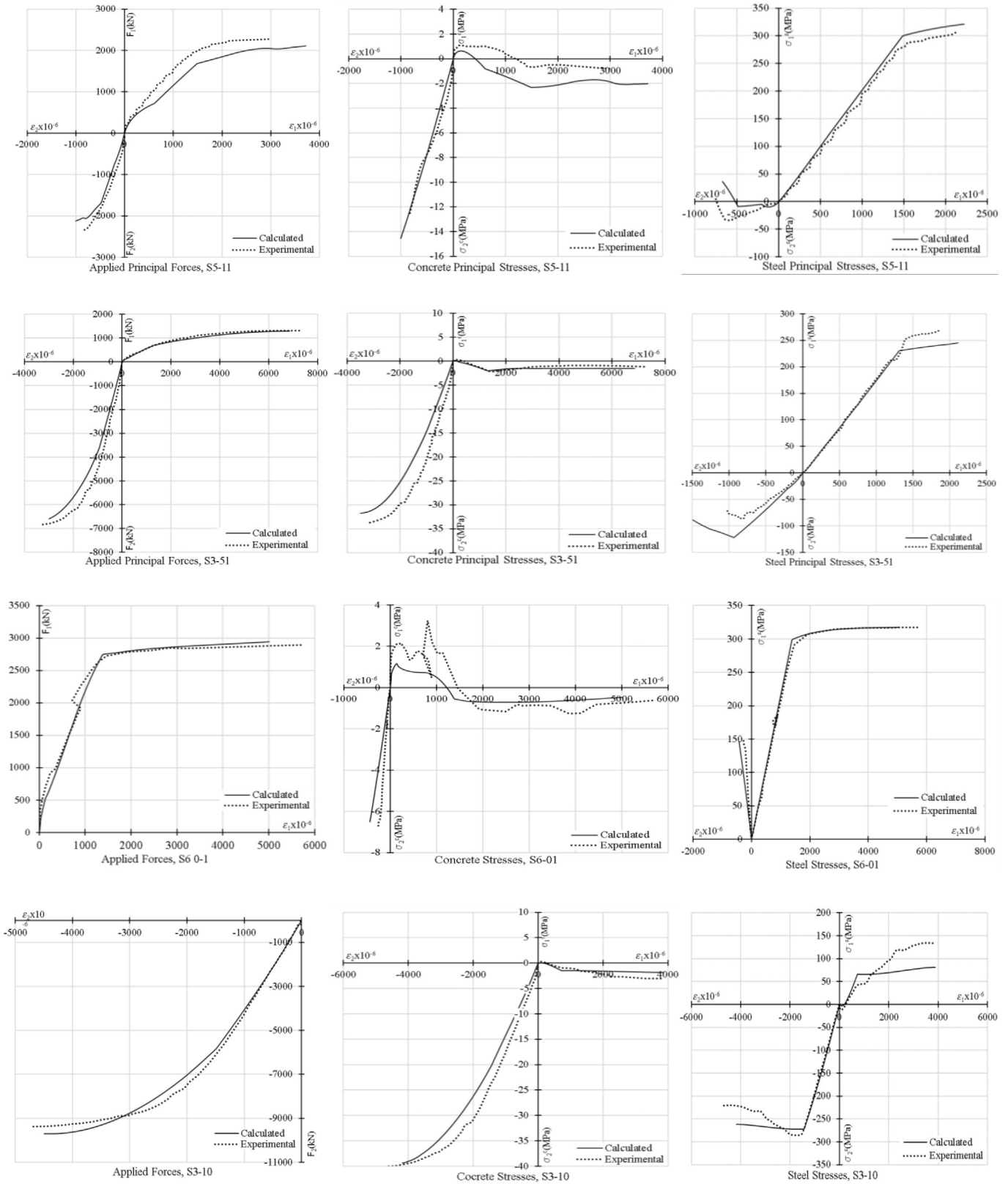
Fig. 13. Comparison of experimental and calculated results.

Fig. 8 illustrates the determination method for the unloading stiffness of the concrete after cracking in principal tensile direction, for which the analytical expression (Eq. (25)) proposed by Belarbi and Hsu [11] and Pang and Hsu [12] is adopted. Fig. 8 shows the curve expressed by Eq. (25). The stiffness at any point along this curve is given by Eq. (26). However, this stiffness should be modified as it does not account for the confinement in the perpendicular direction-2. As confinement tends to improve the stiffness of the concrete, the unloading stiffness is assumed to be 10 times the stiffness given by Eq. (26). The modified stiffness is expressed as Eq. (27) and also
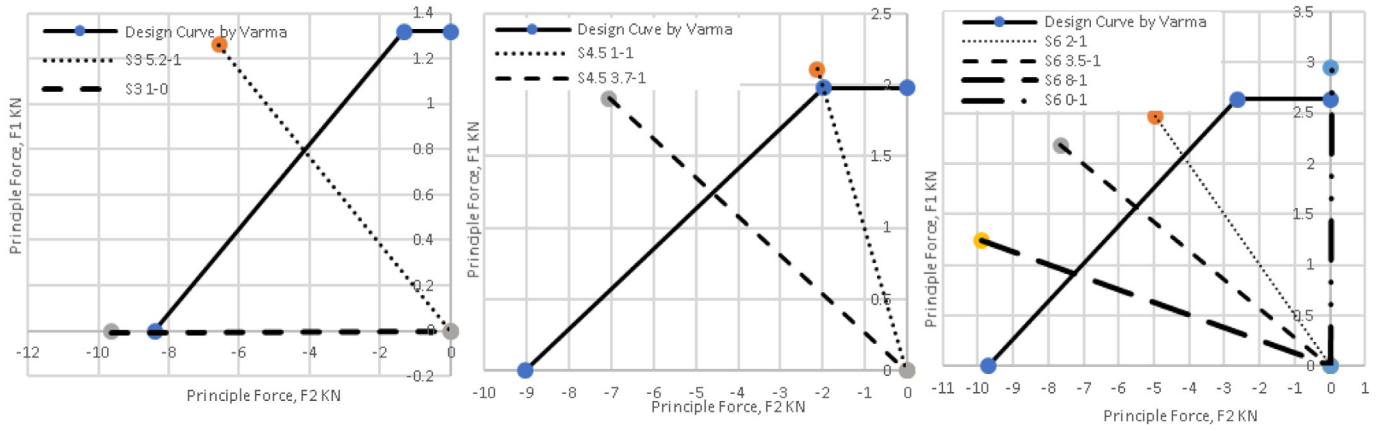
Fig. 14. Comparison of ultimate strengths with design curve by Varma et al. [5].

shown in Fig. 8 as line CA. Therefore, after point c in Fig. 7, the uniaxial stiffness can be determined by Eq. (27) with ε_1 at each loading step. With increasing damage of the concrete, ε_1, the stiffness E_c' deteriorates as shown in Fig. 8 as line CA' and CA".

$$d\sigma_1^c = E_{cr}' d\bar{\varepsilon}_1^c \tag{27}$$

where $E_{cr}' = 4f_{cr}\dfrac{\varepsilon_{cr}^{0.4}}{\varepsilon_1^{1.4}}$ is unloading stiffness of the cracked concrete.

On the other hand, if the loading condition changes and the strain ε_1^{cf} caused by the confining stress becomes less than the strain ε_1^T caused by applied tensile stress, the uniaxial tensile strain may start increasing again. This particular condition was observed due to the change in the loading condition of concrete caused by the yielding of steel plates as shown by point A in Fig. 7. This is analogous to the reloading of the concrete in the tensile direction. The reloading stiffness is assumed to be the same as the unloading stiffness. Therefore, a complete uniaxial stress-strain relationship of concrete in tension and under confinement can be represented by Fig. 7 and above equations.

5.2. Concrete in compression

Uniaxial stress-strain relationship of plain concrete can be represented by a parabolic curve as Eq. (28).

$$\sigma_2^c = f_c'\left[2\frac{\bar{\varepsilon}_2^c}{\varepsilon_o} - \left(\frac{\bar{\varepsilon}_2^c}{\varepsilon_o}\right)^2\right] \tag{28}$$

In SCS, core concrete exhibits a peculiar behavior under shear. Concrete softens under shear due to the presence of tensile stress in the perpendicular direction of applied compressive stress. Softening is a well-understood phenomenon in RC and can be expressed as a function of damage parameter [2]. However, in SCS, as explained, a confining phenomenon may appear along with the softening and may dominate the softening effect in favorable conditions. As observed from the analysis of experimental data, the presence of steel plate reinforcement may not only suppress the softening phenomenon of concrete but, under larger compression to tension ratio, may also enlarge the peak stress point. That is to say, core concrete can exhibit a confining behavior in SCS. Eq. (29) represents a modified stress-strain relationship for concrete in direction-2. On the basis of experimental results of SCS panels, a peak stress modification factor ζ and a peak strain modification factor ξ is proposed. These factors are presented as functions of a combined effect of softening and confining of the concrete core in Eq. (30).

$$\sigma_2^c = \zeta f_c'\left[2\frac{\bar{\varepsilon}_2^c}{\xi\varepsilon_o} - \left(\frac{\bar{\varepsilon}_2^c}{\xi\varepsilon_o}\right)^2\right] \tag{29}$$

where ζ is a modification parameter for peak stress and ξ is a modification parameter for peak strain.

$$\zeta = f_1(\sigma_C^1)\ f_2(\varepsilon_1) \tag{30}$$

To quantify the confinement effect, Guo's [13] chart for triaxial compressive strength of concrete as shown in Fig. 9 is adopted. The chart gives the variation of normalized maximum principal compressive stress $\dfrac{\sigma_{III}}{f_c'}$ with respect to the ratio of intermediate to maximum principal compressive stress $\dfrac{\sigma_{II}}{\sigma_{III}}$ for increasing ratio of minimum to maximum principal compressive stress $\dfrac{\sigma_I}{\sigma_{III}}$. In the experimental data, upper bounds for the parameters were observed as $\dfrac{\sigma_I}{\sigma_{III}} \leq \dfrac{\sigma_{II}}{\sigma_{III}} < 0.15$. Within this limit, a linear approximation of the chart for biaxial stress state is shown in Fig. 10. The variation of $\dfrac{\sigma_I}{\sigma_{III}}$, which is shown by dotted lines in Fig. 10, can be approximated by a straight line as expressed in Eq. (31). The application of the Eq. (31) is, however, limited to the confinement provided by the shear studs and cross ties used in Huang's [8] experiment. For a different density of shear studs and cross ties, Eq. (31) can be modified using the chart in Fig. 9 or a similar chart for concrete triaxial compressive strength given by other researchers. Therefore, the amount of confinement can be estimated by Eq. (31).

$$\frac{\sigma_c^2}{-f_c'} = \left(1 - 12\frac{\sigma_C^1}{f_c'}\right) = f_1(\sigma_C^1) \tag{31}$$

$$f_2(\varepsilon_1) = \left(\frac{1}{\sqrt{1 + 200\varepsilon_1}}\right) \tag{32}$$

$$\xi = 2\zeta \tag{33}$$

Softening effect, Eq. (32), is expressed as a function of principal tensile strain. In RC, Belarbi and Hsu [13] confirmed that the principal tensile strain is the primary factor that dominates the softening coefficient and it must decrease with an increase in the severity of the cracking. A similar concept is put forward for SCS. However, instead of uniaxial strain, the biaxial strain has been used to formulate the softening effect because uniaxial principal tensile strain, in SCS, decreases to zero and might become compressive due to the confinement.

Based on experimental results, for simplicity, the strain modification factor is assumed to be 2 times the stress modification factor as represented in Eq. (33).

6. The solution algorithm

An iterative procedure to analyze the SCS 2D panel is shown in the flowchart in Fig. 11. For each selected value of ε_2, a value for ε_1 is assumed and the uniaxial strains of concrete are calculated using Eqs. (19) and (20). Then, steel stresses are calculated using Eqs. (6) and (14). Similarly, concrete stresses are calculated using Eqs. (23),(24),(27), and (29). Using steel and concrete stresses, panel stresses σ_1 and σ_2 can be determined from Eqs. (2) and (3). With known panels stresses, their ratio σ_2/σ_1 is compared with the ratio of applied load $n = F_2/F_1$, where F_2 and F_1 are applied compressive and tension loads respectively. If the difference of calculated ratio and the ratio of applied loads is within an acceptable range, then the calculated stresses and assumed strain are recorded and the process is repeated with an increment of strain $d\varepsilon_2$. And, if the difference is large, then ε_1 is incremented by $d\varepsilon_1$ and the process is repeated until the difference reaches within the range. Stresses of panel, concrete and steel element are calculated for increasing ε_2. When the compressive strain reaches its peak ε_p, the procedure is stopped.

7. Results and discussion

Experimental results of the SCS panels under biaxial loading is compared with the calculated results of the iterative procedure. Details of the test specimens are given in Table 1. All specimen panels were designed with a size of 800 mm × 800 mm × 260 mm core concrete and with a varying thickness of reinforcing plates. To observe the behavior of the panel under different loading conditions, the specimens were loaded proportionally with a wide range of compression to tension ratios C/T.

Calculated results agree well with the experimental results in all panels as shown in Fig. 12 and Fig. 13. A small deviation in concrete stress in tensile direction is because of the assumptions made while establishing the stress-strain relationship of the concrete in tension. As strain modification factor was assumed an average of 2 times the stress modification factor, the calculated peak compressive strain has slightly deviated from the experimental compressive peak strain in some panels. A small deviation in concrete and steel plate behavior was ignored because the predicted load-deformation behavior of all panels agrees very well with the experimental results.

Failure of an SCS panel can be either tension-controlled or compression-controlled. When concrete reaches its peak compressive strength in principal compressive direction before the yielding of steel in principal tensile direction, it is said to be a compression-controlled panel. Whereas, when steel yields in principal tensile direction before concrete reaches its peak compressive strength in principal compressive direction, it is said to be a tension-controlled panel. All tested panels were found to be compression controlled except panels S6–01 and S6–21, which were tension controlled. The ultimate strength of all panels calculated by the iterative procedure is compared with the design curve of SCS composite wall panels proposed by Varma et al. [5] in Fig. 14. The design curve was shown quite conservative compared to the nonlinear finite element analysis curve proposed by them [5] because it did not consider the flow of steel plate after the yielding. Moreover, the design curve only considers 85% of the design concrete strength f_c', which is very conservative in the case of SCS as the concrete stress was observed to exceed f_c' in panels with high compression to tension load ratio. Hence, the anchor point marking the strength in compression and in tension in the design curve lacks the influence of the plastic flow of the steel plate.

The design curve limits the capacity of the SCS wall panels to its tensile strength for all principal forces loading ratio F_2/F_1 less than and equal to 1. SCS wall panels with a loading ratio of more than 1 such as S6 2–1 was found to have a tensile failure. So, the anchor point marking the shear strength, which limits the capacity of the SCS wall panel to its tension capacity, is found to extend as the concrete does not reach its

capacity. A modified analytical curve is proposed by Song et al. [14], which incorporates such considerations.

8. Conclusion and recommendations

To analyze an SCS panel, an iterative procedure was developed by introducing a modified constitutive relationship of concrete. The model was then verified with the experimental results of SCS wall panels. The model proves effective to predict the behavior of the SCS panel. The ultimate capacity calculated was found to be higher than the conventional design methods due to the previously mentioned reasons.

The modified stress-stress relationship of concrete presented in this paper can be extended to incorporate the post-peak behavior. A simplified constitutive relationship in tension was assumed to simulate the confined behavior of concrete in principal tensile direction, which deviates a little from the experimental results. So, a more accurate analytical relationship can be proposed for concrete in tension. For concrete in compression, the strain modification factor was assumed an average of 2 times the stress modification factor. This assumption leads to a small deviation in peak strain in some panels. A detailed study is needed to develop a relationship for the strain modification factor as a function of its influencing factor.

Declaration of Competing Interest

The authors declare that they have no known competing financial interests or personal relationships that could have appeared to influence the work reported in this paper.

References

[1] J.B. Yan, X. Liu, J. Liew, M. Zhang, Steel–concrete–steel sandwich system in arctic offshore structure: materials, experiments, and design, Mater. Des. 91 (2016) 111–121.
[2] T.T. Zhu, R.R. Hsu, Softened membrane model for reinforced concrete elements in shear, ACI Struct. J. 99 (4) (2002) 460–469.
[3] M. Ozaki, S. Akita, H. Osuga, T. Nakayama, N. Adachi, Study on steel plate reinforced concrete panels subjected to cyclic in-plane shear, Nucl. Eng. Des. (2004) 225–244.
[4] N.E.A. Suzuki, H. Akimaya, M. Narikawa, K. Hara, M. Takeuchi, I. Matsuo, Study on a concrete filled steel structure for nuclear power plants part 4: analytical method to estimate shear strength, SMiRT13, Porto Alegre, Brazil, 1995.
[5] A.H. Varma, S.R. Malushte, K. Sener, Z. Lai, Steel-plate composite (SC) walls for safety related nuclear facilities: design for in-plane and out-of-plane demands, SMiRT, New Delhi, 2011.
[6] Frank J. Vecchio, Ian McQuade, Towards improved modeling of steel-concrete composite wall elements, Nucl. Eng. Des. (2011) 1–3.
[7] F. Vecchio, Distributed stress field model for reinforced concrete: formulation, ASCE J. Struct. Eng. (2000) 1070–1077.
[8] C.J. Huang, S.J. Chen, Y.B. Leng, C.H. Qian, X.B. Song, Experimental research on steel-concrete-steel sandwich panels subjected to biaxial tension compression, J. Constr. Steel Res. 162 (2019) 105725p. In progress.
[9] R.R.H. Zhu, T. Hsu, Poisson effect in reinforced concrete membrane elements, ACI Struct. J. (2002) 631–640.
[10] Y.M. Thomas, T.C. Hsu, Unified Theory of Concrete Structures, Jhon Wiley & Sons Ltd., 2010.
[11] A. Belarbi, T. Hsu, Conctitutive laws of concrete in tension and reinforcing bars stiffened by concrete, ACI Srtuct. J. (1994) 465–474.
[12] X. Pang, T. Hsu, Behaviour of reinforce concrete menbrane elements in shear, ACI Struct. J. (1995) 665–679.
[13] T.T.C.H. Abdeldjelil Belarbi, Constitutive Laws of softened concrete in biaxial tension-compression, Ame. Concrete Inst. Struct. J. (1995) 562–572.
[14] W. Hailin, C. Meng, G. Honghui, X.B. Song, A failure criterion for steel-concrete composite walls, The International Conference on Sustainable Development of Critical Infrastructure, Shanghai, 2004.
[15] W.-F. Chen, Constitutive Equations for Engineering Materials, vol. 1, John Wiley & Sons, Inc, New York, 1994.